Preparation and Characterization of Lanthanum Oxide doped Barium Zirconate Titanate ($BaZr_{0.1}Ti_{0.9}O_3$; BZT) Ferroelectric Glass Ceramics

AVINASH MEHER

Department of Ceramic Engineering
National Institute of Technology, Rourkela
Rourkela - 769008, India

Preparation and Characterization of Lanthanum Oxide doped Barium Zirconate Titanate ($BaZr_{0.1}Ti_{0.9}O_3$; BZT) Ferroelectric Glass Ceramics

Thesis submitted in

June 2015

To the department of

Ceramic Engineering

of

National Institute of Technology, Rourkela

In partial fulfilment of the requirements

For the degree of

Bachelor of Technology

By

Avinash Meher

(Roll 111CR0101)

Under the supervision of

Prof. Partha Saha

Department of Ceramic Engineering
National Institute of Technology, Rourkela
Rourkela - 769008, India

Certificate

This is to certify that the work in the thesis entitled as **"Preparation and Characterization of Lanthanum Oxide doped Barium Zirconate Titanate ($BaZr_{0.1}Ti_{0.9}O_3$; BZT) Ferroelectric Glass Ceramics"** by Avinash Meher, with roll number 111CR0101, is a record of an original experimental work carried out by him under my supervision and guidance in partial fulfilment of the requirements for the award of the degree of Bachelor of Technology in Ceramic Engineering.

Dr. Partha Saha
Assistant Professor
Department of Ceramic Engineering
National Institute of Technology, Rourkela

ACKNOWLEDGEMENT

I would like to express my deep perception of appreciation to all of them without whom this particular project of mine would have been incomplete. Principally I would really like to say thanks to my supervisor, Prof. Partha Saha, Department of Ceramic Engineering, National Institute of Technology, Rourkela, for his incalculable efforts for this project. He ignited me personally to be effective on the subject as well as provided useful information which assisted me to perform the work in a timely manner.

I am thankful to every one of my professors at Department of Ceramic Engineering, NIT Rourkela for helping me the fundamental information about the subject that altogether profited me doing my endeavour and also achieving my target. I would like to express profound gratitude to our staff members at National Institute of Technology, Rourkela for helping during the work as and when required.

I moreover express profound gratitude to my companions and in addition associates who have given their own particular time whenever required. Their commitment is without a doubt a major boost. At last, I take this opportunity to express profound gratitude to my parents, who have been a wellspring of inspiration and also motivation as I would see it, for their gratefulness, which for the most part is a tremendous directing push for accomplishment.

CONTENTS

LIST OF FIGURES:

LIST OF TABLES:

ABSTRACT

[($BaZr_{0.1}Ti_{0.9}O_3$]-[$2SiO_2$-B_2O_3]-[K_2O] based borosilicate glass with and without 0.1 mol % La_2O_3 was successfully developed by melt-quench method. XRD and FTIR spectra of the glass sample shows broad peaks ~24-35˚ (2θ value) which is due to the formation of amorphous borosilicate phase and presence of stretching and deformation vibrations of B-O-Si linkage and Si–O–Si bridges, respectively. Differential scanning calorimetry (DSC) of glass samples reveals that addition of 0.1 mol % La_2O_3 elevates the onset of crystallization temperature from ~560˚C to ~628˚C. Controlled crystallization of the glasses at 800˚C for 3h leads to the formation of fresonite ($Ba_2TiSi_2O_{8)}$ phase. SEM-EDS analysis of the un-doped glass-ceramic sample shows the formation of micron sized L-shaped and needle shaped crystals. However, addition of 0.1 mol % La_2O_3 modify the L-shaped crystal structure to blocky globular crystals. Dielectric measurements shows that addition of 0.1 mol % La_2O_3 increases the dielectric constant from ~45 to ~125.

1. INTRODUCTION

1.1 Barium Titanate

Barium Titanate ($BaTiO_3$) is widely used in the electronic industry because of its ferroelectric properties finding extensive applications as dielectric material in piezoelectric actuator, multilayer ceramic capacitors, embedded capacitance as positive temperature coefficient of resistivity sensors and also used in printed circuit boards. $BaTiO_3$ is an inorganic compound it has perovskite structure and it has ferroelectric properties. Ferroelectric ceramics have wide range of applications in the electronic industry because it has high dielectric permittivity.

Barium Zirconate Titanate (BZT) is an important species of the family of $BaTiO_3$. Its potential applications are such as DRAM for memory application, tunable microwave devices, piezoelectric transducers, and electrical energy storage units. $BaZr_xTi_{1-x}O_3$ (BZT) ceramics are interesting materials for being used as dielectrics in commercial capacitor applications. They present high voltage resistance, high dielectric constant, and composition- dependent Curie temperature (T_C). It has been reported that $BaZr_xTi_{1-x}O_3$ exhibits better temperature stability than $Ba_{1-x}Sr_xTiO_3$ in paraelectric state. A common way to improve the material performance is by impurity-doping in BZT electroceramics [1].

The temperature characteristic of BZT is smoothened by increasing dependency of permittivity on temperature. In $BaZr_xTi_{1-x}O_3$ (BZT) when the Zr content very low (10 at %) it shows normal ferroelectric behavior. The dielectric data of $BaZr_xTi_{1-x}O_3$ (BZT) ceramic suggest that a normal ferroelectric behavior is observed for $0<x<0.1$, diffused phase transition for $0.1<x<0.2$, relaxor characteristic for $0.2<x<0.5$. The degree of diffuses of the ferro –para phase transition increases with Zr addition. For $x>0.5$ it is no more ferroelectric. Recently discovered BZT ferroelectrics have been chosen over BST based ferroelectrics for fabrication capacitors.

1.2 Perovskite structure

Any material with the same type of crystal structure as calcium titanium oxide ($CaTiO_3$) is said to have perovskite structure. Examples of materials having perovskite structure- Barium titanate ($BaTiO_3$), Lead Zirconate Titanate (PZT), Lead Lanthanum Zirconate Titanate (PLZT), Lead Titanate ($PbTiO_3$), and Potassium Niobate ($KNbO_3$). The name Perovskite was given after the mineralogist L.A. Perovskite who first discovered it the Ural mountain of Russia. The general formula of Perovskite is ABO_3, where A & B are two cations of different sizes and O is oxygen that bonds with both the cation. The A atom which are at the cube corner positions are larger in size than the B atoms that are in the body center position and oxygen atoms are at face centered position of a cube. Perovskite structure is adopted by many oxides that have the chemical formula (ABO_3).

B atoms are transition metals and have higher charge than A atoms (A:Na^+,K^+,Ca^{2+},Ba^{2+},Pb^{2+} etc, B:Ti^{4+},Zr^{4+},Sn^{4+},Nd^{5+},Ta^{5+},W^{6+} etc.).

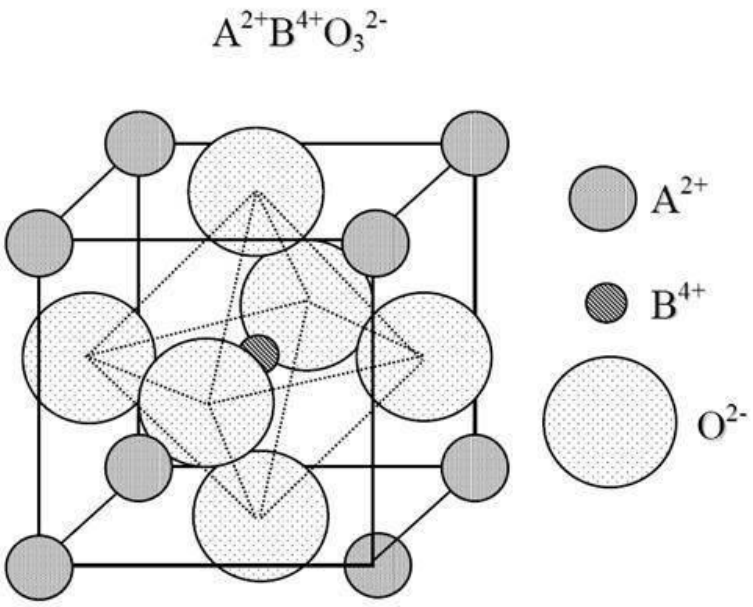

Fig. 1.2.1 A cubic ABO_3, perovskite type unit cell.

Barium titanate ($BaTiO_3$), the first ceramic material in which ferroelectric behavior was observed, was reported in the year 1945, [2]. Barium titanate ($BaTiO_3$) has now become one of the most extensively studied ferroelectric materials for its applications in electronic industries because it has a much simpler structure (perovskite), better ferroelectric properties, chemical stability and mechanical stability [3]. In addition to that, chemical and mechanical stability, at and above room temperature is observed and can be easily fabricated and used in the form of polycrystalline materials.

The discovery of ferroelectricity in $BaTiO_3$ [3], has given birth to a large number of ABO_3 type perovskite ferroelectrics, where A site can have a monovalent cation, divalent cation or trivalent cation and B site can have a trivalent cation, tetravalent cation or pentavalent cation. It has been found that in ideal ABO_3 perovskite structure corner is shared by $[BO_6]$ octahedra and the A cation has a 12-fold coordination at the center of the cube and it is surrounded by eight $[BO_6]$ octahedra. The O anion is often oxygen but can be replaced by fluorine or chlorine ion. But this ideal structure is not common and displays many types of structural instabilities in the various materials. The reason for enhanced ferroelectric properties is reduced symmetry of the distorted crystal structure of the perovskite. These may lead to displacements of the cations as well as rotations and distortions of the oxygen octahedral from their original sites. These type of instabilities accounts for the rich variety of antiferroelectric (AFE) and ferroelectric (FE) behaviors.

Table. 1 Roles of different phases

Phases	**Role of phases**
$BaZrTiO_3$	Forms dielectric phase
SiO_2-B_2O_3	Glass former
K_2O	Glass intermediate
La_2O_3	Acts as dopant

1.3 Role of La_2O_3 dopant

For crystallization of glass ceramics lanthanum oxide (La_2O_3) is used because it acts as a nucleating agent. This can be observed by the crystallization of doped glass takes place at low temperature compared to the base glass and this increases the value of dielectric constant. Lanthanum oxide doped glass ceramics also have higher density and they affect the tetragonality of BZT. In BZT glass ceramics the value of energy density increases to 2.56 times by the addition of La_2O_3. In the modification of crystal structure (tetragonality) of BZT phase La^{3+} ions plays a major role as it gets diffused into the structure.

In La_2O_3-doped $BaTiO_3$ ceramics replacement of Ba^{2+} on the A-site by La^{3+} (La^{3+} ion is too large to replace Ti on the B-site) occur but La^{3+} has higher valence so this causes charge imbalance which should be compensated either by electrons (electronic compensation) or cation vacancies on the A or B site (ionic compensation) [4]. In addition to direct donor dopant specifically at low donor concentration, is considered to be the mechanism of the charge compensation which exhibits semi-conductive properties.

2. LITERATURE REVIEW

Xiujian Chou *et al.* [5] studied La_2O_3-doped barium zirconate titanate $(Ba_{1-x}La_x)Zr_{0.2}Ti_{0.8-x/4}O_3$ ceramics fabricated by conventional solid-state route. They investigated that the ferroelectric relaxor behavior and dielectric properties of $(Ba_{1-x}La_x)Zr_{0.2}Ti_{0.8-x/4}O_3$ ceramics is caused by substitution of La^{3+} ions in the A-site for Ba^{2+} ions. But it enters the unit cell maintaining the perovskite structure of solid solution which enhances the ferroelectric relaxor behavior. The substitution of barium (Ba) sites by lanthanum (La) in $(Ba_{1-x}La_x)Ti_{1-x/4}O_3$ ceramics tends to shift the Curie peak (T_C) toward low temperature.

With the increase in value of x the T_C (Curie temperature) of $(Ba_{1-x}La_x)Zr_{0.2}Ti_{0.8-x/4}O_3$ ceramics shifts to lower temperature and thus the dielectric constant can be adjusted from thousands to hundreds. La-doping is done to reduce the dielectric loss of $(Ba_{1-x}La_x)Zr_{0.2}Ti_{0.8-x/4}O_3$ ceramics. The tunability of paraelectric phase $(Ba_{1-x}La_x)Zr_{0.2}Ti_{0.8-x/4}O_3$ ceramics is associated with the size and quantity of cluster and micro-domain. And it decreased with increase of La_2O_3 dopant. When the $x \geq 0.04$ in a (dc applied) electric field of 20 kV/cm the tunability of $(Ba_{1-x}La_x)Zr_{0.2}Ti_{0.8-x/4}O_3$ ceramics would disappear. The $(Ba_{1-x}La_x)Zr_{0.2}Ti_{0.8-x/4}O_3$ ceramics for (x = 0.01–0.02) having a low dielectric loss, suitable dielectric constant and high tunability could be used as tunable ceramic capacitors and in tunable microwave device applications.

Feri Adriyanto *et al.* [6] studied and demonstrated Pentacene-based organic thin-film transistors with solution-processed barium zirconate titanate dielectric layers. According to the programming/erasing operations the devices were having remarkable memory characteristics, such as reversible threshold voltage shifts and nondestructive readout. The devices exhibited reversible shifts in threshold voltage of 1.32 V by a low erasing processes (±10 V) and electrical programming. The measurement of retention time shows that the stored information could be maintained for a significantly long duration $>10^3$ s. By using the repeated programming/erasing operation they perform the endurance test for 50 times. A proposed possible mechanism of these characteristics could be the trapping and de-trapping of charge carriers in the BZT layers. They were able to improve the memory performance of the devices, by fabrication of devices by solution process which makes them probable for large-area and economical nonvolatile memory applications.

Tanmoy Maiti *et al*. [7] studied the effects addition of Zr in the relaxor behavior of $Ba(Zr_xTi_{1-x})O_3$ system. They successfully prepared compositions of $Ba(Zr_xTi_{1-x})O_3$ (BZT) with the

value of x ranging from 0.35 to 1.00 using the conventional solid-state method. Dielectric, pyroelectric and thermal strain measurements have been done from very low cryogenic temperature to high temperatures. They were also able to develop a complete phase diagram of lead-free relaxor ferroelectrics of barium zirconate titanate, $Ba(Zr_xTi_{1-x})O_3$ system with compositions ($0.00<x<1.00$) based on their dielectric behavior.

Barium zirconate titanate, $Ba(Zr_xTi_{1-x})O_3$ system depending on the value of x shows the properties extending from simple dielectric (pure $BaZrO_3$) to polar cluster dielectric for higher values of x, relaxor ferroelectric, second order like diffuse phase transition, ferroelectric with pinched phase transitions, and then to proper ferroelectric properties like pure $BaTiO_3$. The $BaZr_xTi_{1-x}O_3$ having compositions ($x \geq 0.80$) start showing polar-cluster like behavior referring to the thermal hysteresis in dielectric behavior and DC field dependent dielectric studies with the substitution of Ti^{4+} ion in the $BaZrO_3$ matrix. In the nonpolar matrix of $BaZrO_3$ beyond an optimum content of polar $BaTiO_3$ probably a critical size and distribution density of the polar regions are reached when polar cluster like $Ba(Zr_xTi_{1-x})O_3$ ceramics start showing the relaxor-like behavior for compositions having ($x \leq 0.75$). $BaZr_xTi_{1-x}O_3$ depending on the value of x has properties different than the conventional solid solution and those do not follow the simple mixing rules considering the properties of the constituents, $BaZrO_3$ and $BaTiO_3$. In this context the $BaZr_xTi_{1-x}O_3$ relaxor compositions can be classified as a very good example of metamaterials where the polar clusters result in the relaxor materials with the unusually enhanced dielectric properties not present in either of the end member compositions.

F. Mouraa *et al*. [8] studied the changes in the relaxor behavior of BZT ceramics upon addition of Zr. They prepared barium zirconium titanate (BZT) ceramics by mixed oxide method. This method was used to obtain single phase barium zirconium titanate (BZT) powders at 1200˚C

for 2 h. The increase in Zr content affects the crystal structure which was observed by performing Raman spectroscopy. It was found that the temperature for transition from ferroelectric to paraelectric phase decreases when Zr content equal to 15 mol.%. Because of the Zr content, they observed a typical relaxor behavior. A decrease in the dielectric permittivity and remnant polarization with the increase of Zr content the relaxor property was reduced which is caused by changes in crystal structure.

S. Sarangi *et al.* [9] studied the frequency and temperature dependence dielectric behavior of barium zirconate titanate (BZT) nanocrystalline powder. They characterized the nano-ceramic by X-ray diffraction (XRD), scanning electron microscopy (SEM), impedance spectroscopy and dielectric study. The presence of tetragonal structure at room temperature was confirmed by XRD analysis so the BZT ceramic should have ferroelectric properties. Microstructural analysis was done by scanning electron microscope to show that the particle size is very small in nanometer range. A normal ferroelectric behavior in the material is observed in the dielectric measurement done with respect to changing temperature. The electrical parameters such as the real and imaginary part of impedance was studied by impedance spectroscopy. This method was also used to study ac/dc conductivity as a function of both frequency and temperature. It has been found that the electrical relaxation process occurring in the material depends on the change in temperature.

3. OBJECTIVES

Objective of the present work is following

1. Preparation of $BaZr_{0.1}Ti_{0.9}O_3$ base glass and 0.1 mol.% La_2O_3 doped glass.
2. Perform FTIR (Fourier Transform Infrared Spectroscopy) on the base glass to identify the bonding modes of different glass forming constituents.
3. Determine the crystallization temperature of ferroelectric phase from the DSC study.

4. Preparation of glass ceramic samples by thermal treatment above crystallization temperature.
5. Microstructural analysis of glass and glass ceramic samples using XRD, SEM-EDS, X-ray mapping.
6. Measurement of density of glass and glass ceramic samples.
7. Dielectric measurement of glass ceramics as a function of both frequency and temperature.

4. EXPERMENTAL METHODS

4.1 PREPARATION OF GLASS

The fabrication of glass ceramic involves the production of a homogenous glass and then conversion of this glass ceramic in to a microcrystalline glass ceramic by application of controlled heat treatment process. Reagent grade chemicals such as $BaCO_3$, ZrO_2, H_3BO_3, TiO_2, K_2CO_3, SiO_2, and La_2O_3 shown in **Table 2** were used for the preparation of glass as well as glass ceramic samples.

Table 2 List of chemicals used in the present study

Reagent grade	Molecular weight (g/mol)	Purity (%)	Company name
$BaCO_3$	197.34	97	Merck
ZrO_2	123.2	99	Loba Chemie
TiO_2	79.866	≥99	Merck
SiO_2	60.08	99.8	TRL, Belpahar
H_3BO_3	61.83	99.5	Merck
K_2CO_3	138.21	99.9	Merck
La_2O_3	325.81	99	Loba Chemie

The flow chart shown in **Fig. 4.1** displays the steps used to prepare the glass samples**.** Stoichiometric amount of raw materials were weighed and mixed in an agate mortar using acetone as mixing media. The mixed powder was transferred in a platinum crucible and melted at 1350˚C using an electric furnace. The melt was held at 1350˚C for 2h for homogenization before pouring onto a pre-heated steel mold at room temperature. The glass samples were annealed at 600˚C for

3h in order to remove residual stresses developed due to thermal gradient. Further, the glass samples were crystallized at elevated temperature according to the DSC study**.**

Fig. 4.1 Flow Chart for Preparation of Glass

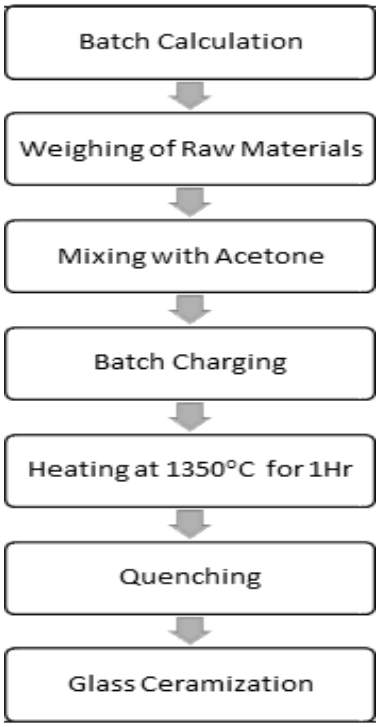

Batch Calculation

Table 3 and 4 shows the batch calculation used for preparing glass samples of batch I, II & III.

Table. 3 Batch calculation for 100g batch, Composition- [($BaZr_{0.9}Ti_{0.1}O_3$]-[$2SiO_2$-B_2O_3]-[K_2O]

Reagent grade	Molecular weight (g/mol)	Mol. % required	Formula weight (g/mol)	For 100g batch (g)
$BaCO_3$	197.34	1	663.262	29.75
ZrO_2	123.2	0.1		1.857
TiO_2	79.866	0.9		18.117
SiO_2	60.08	2		10.84
H_3BO_3	61.83	2		18.594
K_2CO_3	138.21	1		20.838

Table 4 Batch calculation for 50g batch, Composition- [Ba $Zr_{0.9}Ti_{0.1}O_3$]-[$2SiO_2$-B_2O_3]-[K_2O]-0.1 mol % [La_2O_3]

Reagent grade	Molecular weight (g/mol)	Mol % required	Molecular weight (g/mol)	For 50g batch (g)
$BaCO_3$	197.34	1	695.843	14.17
ZrO_2	123.2	0.1		0.8853
TiO_2	79.866	0.9		5.165
SiO_2	60.08	2		8.635
H_3BO_3	61.83	2		8.86
K_2CO_3	138.21	1		9.93
La_2O_3	325.81	0.1		2.34

For Batch I:

For melting Batch I, 100g batch was prepared and transferred into a cylindrical alumina crucible. The alumina crucible was placed in another crucible with alumina powder to hold the cylindrical crucible. The batch was melted in a raising hearth electric furnace at 1350˚C. The liquid melt was maintained inside the furnace for 2h for homogenization and refining, then it was poured on a pre-heated graphite plate.

For Batch II & III:

For melting Batch II and III 20g batch was prepared and then transferred in a platinum crucible. The batches were melted in a raising hearth electric furnace. The melt is maintained inside the furnace for 2 hours for homogenization and refining, then it is poured out into a two piece brass plates while the other plate is immediately pressed over the melt to achieve high rate of cooling.

4.2 PREPARATION OF GLASS CERAMIC

The glass samples were fired at different temperatures obtained from the DSC data. The information we get from the DSC curve is the T_g (glass transition temperature), T_{C1} and T_{C2} (where T_{C1} and T_{C2} are crystallization temperature). Depending upon the information we get from the DSC curve glass ceramization procedure is next followed by heat treatment method. The samples

were kept on an alumina base plate and according to the respective temperatures the samples were heat treated on the basis of the heat treatment schedule.

4.3 MATERIAL CHARACTERIZATION

4.3.1. X-Ray Diffraction (XRD)

For XRD characterization the glass and glass ceramics obtained from different heat treatment schedules were ground to fine powder. The powder was carefully placed on the sample holder and levelled by a glass slide to maintain a uniform level then placed in the XRD (Rigaku Japan/Ultima-IV) machine having the 2θ value from 10-70˚ using the step size 0.05 and CuK_a radiation. And for glass ceramic powder 2θ value 20-70˚ was taken. The XRD data was obtained and by using Origin software XRD graphs were plotted. X'pert HighscorePlus software was used to identify the phases present in the sample. Bragg's law equation-

$$n\lambda = 2dsin\theta$$

Where:- n is the order of diffraction, λ is X-ray wavelength, d is inter-planar spacing and θ is the angle of diffraction

4.3.2. Differential Scanning Calorimetry (DSC)

For DSC characterization the glass obtained from different heat schedules were ground to fine powder. The powder was placed in a small crucible and placed in the sample holder for DSC measurement. The crucible is then loaded into the DSC equipment (Netzsch, Germany, STA449C/4/MFC/G). For base glass samples measurements were taken from room temperature to 700˚C. And for doped glass sample measurements were taken from room temperature to 750˚C with a heating rate of 10˚C/min.

4.3.3 Density measurement

Three glass and glass ceramic samples of each batch was taken for density measurement. Marking was done on every sample, dry weight (D) was measured for each sample. Then they were placed inside a beaker filled with water. The beaker was placed in vacuum chamber for 2 hours. After 2 hours suspended weight (W) and soaked weight (S) was measured. To find Bulk Density of each sample the following formula was used:

$$\text{B.D} = \frac{D}{W-S}$$

4.3.4 Fourier Transformation Infrared Spectroscopy (FTIR)

Infrared spectroscopy is employed to study the molecular and/or atomic structure within a specimen. Only glass samples were used for FTIR analysis, glass powder was prepared for each batch. The powder was mixed with KBr powder and poured into a die punch for hydraulic press to make a pellet (70 to 80) atmospheric pressure was applied to make a pellet. FTIR spectra for the powdered glass specimens mixed with KBr were recorded in 4000-450 cm^{-1} range with a PerkinElmer Spectrum Two (model number 95277) spectrometer.

4.3.5 Polishing of glass ceramic samples for FESEM analysis and Dielectric measurement

Glass ceramic samples were cut to regular shapes (square, rectangle) using a diamond cutter. Then the samples were polished using different sand paper to bring the samples to regular shape. Different sand papers were used are grid 240, grid 320. Different emery paper used were gid 600, grid 1200 for polishing the samples. Further polishing was done on a rotating polishing machine using lapped cloth. Diamond paste (3μm) was applied on lapped cloth. Polishing was done until sample surfaces show mirror-like finish.

4.3.6 Field Emission Scanning Electron Microscope (FESEM)

For FESEM polished glass ceramic samples were used. The samples were mounted on copper stub with the help of Ag paste and sequence was noted. Samples were prepared for SEM

examinations by sputtering Au film onto the polished surfaces of glass ceramic to prevent charge build-up. The photographs of samples were taken at different magnifications. Microstructural analysis of the glass ceramic samples were performed at 15kV using a Field Emission Scanning Electron Microscope (NOVA NanoSEM/FEI).

4.3.7 Dielectric Measurement

Both the surface of glass ceramic samples were polished using sand paper and emery paper for attaining smooth surface to a thickness of 1.4 mm. The electrodes were made by applying Ag-Pd paint on both sides of the samples. The samples were first dried in a drier at 100˚C and then cured at 600˚C for 30 minutes. The dielectric parameters i.e capacitance (C), dielectric loss (D) and conductance (G) were measured as a function of frequency in a locally fabricated platinum sample holder using a HIOKI 3532-50 LCR High Tester. For measurement of dielectric as a function of frequency, (100Hz-1MHz) range of frequency was used. Dielectric constant (ε_r) was calculated from capacitance (C) using the relation;

$$\varepsilon_r = C.\frac{t}{\varepsilon_0 A}$$

where, C is the capacitance, ε_0 is the permittivity of free space (ε_0 = 8.854 * 10^{-12} F/m), A and t are area and thickness of sample in square meter and meter respectively.

5. RESULTS AND DISCUSSION

5.1. X-RAY DIFFRACTION (XRD) OF BASE GLASS AND DOPED GLASS

The glass samples were ground to fine powder for XRD analysis. **Fig. 5.1.1-5.1.3** shows the XRD plot of each samples with the compositions [($BaZr_{0.1}Ti_{0.9}O_3$]-[$2SiO_2$-B_2O_3]-[K_2O] quenched on a preheated plate graphite plate, [($BaZr_{0.1}Ti_{0.9}O_3$]-[$2SiO_2$-B_2O_3]-[K_2O] quenched at room temperature and doped glass [($BaZr_{0.1}Ti_{0.9}O_3$]-[$2SiO_2$-B_2O_3]-[K_2O] - 0.1 mol. % La_2O_3 also quenched at room temperature, respectively. All three XRD pattern shows broad peaks around

~24-35˚ (2θ value) which is due to the formation of amorphous borosilicate phase. The presence of amorphous borosilicate phase confirms formation of desired borosilicate glass.

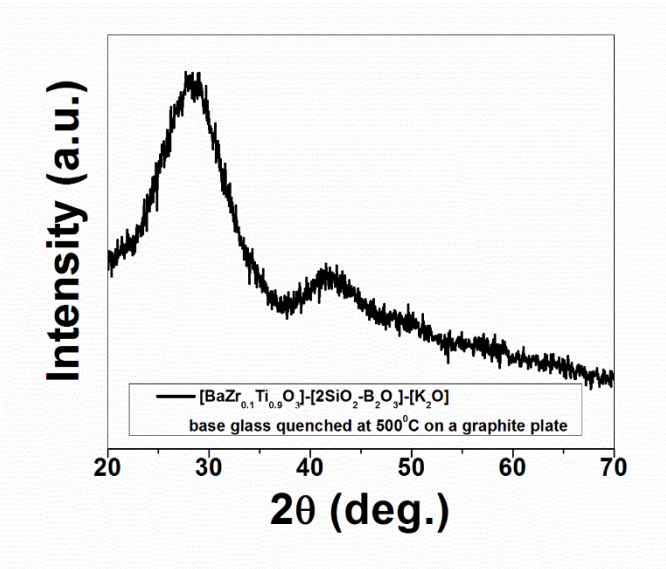

Fig. 5.1.1 XRD analysis of [($BaZr_{0.1}Ti_{0.9}O_3$]-[$2SiO_2$-B_2O_3]-[K_2O] glass sample quenched on pre-heated graphite plate.

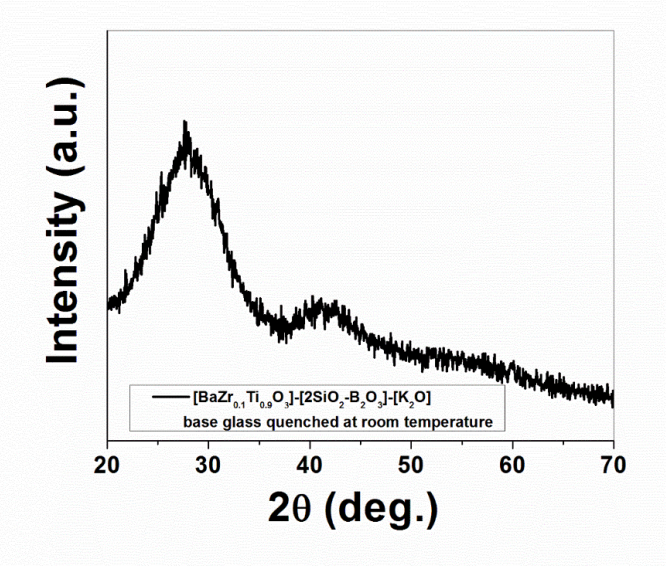

Fig. 5.1.2 XRD analysis of [($BaZr_{0.1}Ti_{0.9}O_3$]-[$2SiO_2$-B_2O_3]-[K_2O] glass sample quenched at room temperature.

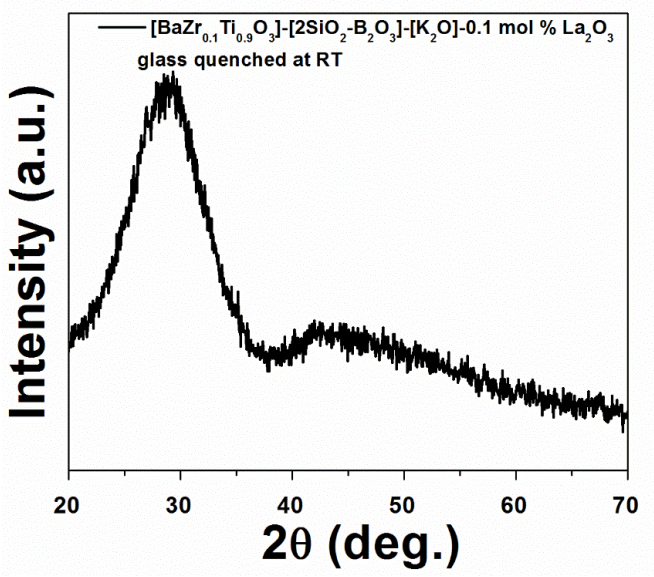

Fig. 5.1.3 XRD analysis of [($BaZr_{0.1}Ti_{0.9}O_3$]-[$2SiO_2$-B_2O_3]-[K_2O]- 0.1 mol. % La_2O_3 doped glass sample quenched at room temperature.

5.2 FOURIER TRANSFORMATION INFRARED SPECTROSCOPY (FTIR)

The FTIR spectrum for the BZT base glass and 0.1 mol.% La_2O_3 doped BZT glass is shown in **Fig. 5.2.1** and **Fig. 5.2.2**. The peaks of the infrared spectroscopy are listed in the **Table 5** and **Table 6,** respectively. The FTIR spectra for these glasses generally consist of broad and diffuse bands in the region 4000-450 cm^{-1}. The transmission band in the wave number range 3436–3456 cm^{-1} observed due to the molecular water present inside the glassy matrix [10]. A possible reason for the presence of O–H bond is the KBr pellet technique. Two absorption bands are also present in the range 1200-1750 cm^{-1} In this wavenumber range peaks are caused due to asymmetric stretching relaxation of the B–O bond of trigonal BO_3 units [11]. Peaks at wavenumber range 900-910 cm^{-1} is caused due to stretching vibrations of B-O-Si linkage [12]. In 707–720 cm^{-1} wavenumber range the peaks are due to the diborate B-O-B link found in the borate glassy network [13]. For base glass sample 460-515 cm^{-1} wavenumber range attributes to deformation vibrations of the Si–O–Si bridges. For doped glass sample 470-520 cm^{-1} is caused due to vibration of Ba^{2+} ion [14].

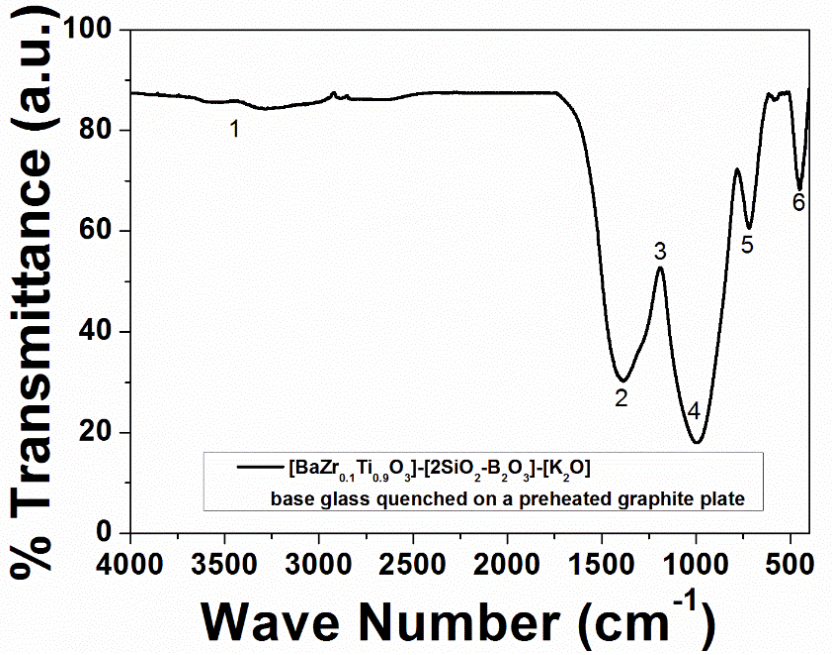

Fig. 5.2.1 FTIR spectra of [($BaZr_{0.1}Ti_{0.9}O_3$]-[$2SiO_2$-B_2O_3]-[K_2O] glass sample quenched at high temp.

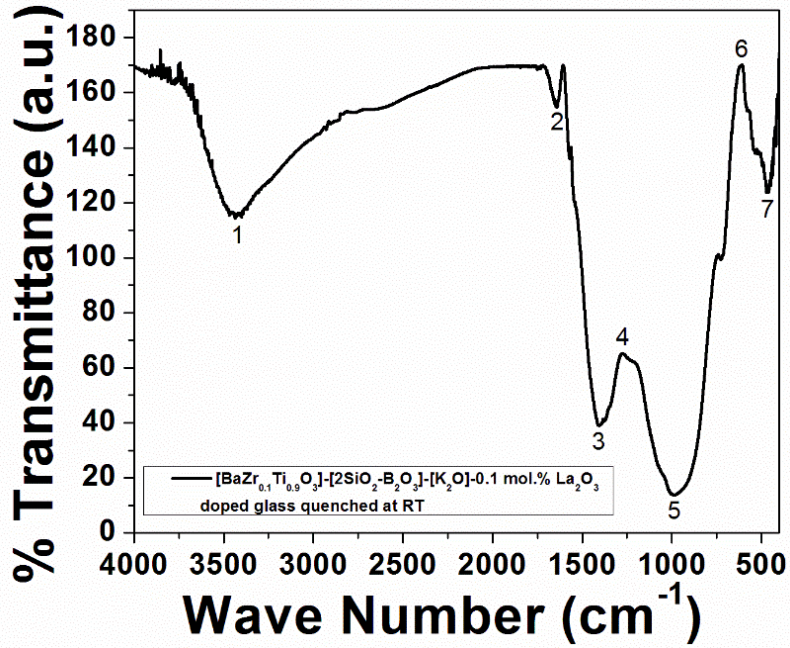

Fig. 5.2.2 FTIR spectra of [($BaZr_{0.1}Ti_{0.9}O_3$]-[$2SiO_2$-B_2O_3]-[K_2O] 0.1 mol. % La_2O_3 glass sample quenched at room temperature.

Table 5 FTIR peaks and characteristics of base glass.

Sl no.	Wavenumber (cm^{-1})	Characteristics
1	3450 - 3470	Stretching of O–H– bond inside the glassy network
2	1200 - 1750	Asymmetric stretching relaxation of the B–O bond of trigonal BO_3 units.
3	1200 - 1750	Asymmetric stretching relaxation of the B-O bond of trigonal BO_3 units.
4	900 - 910	Stretching vibrations of B-O-Si linkage.
5	700 - 720	Bonding of B-O-B linkages (diborate linkage).
6	460 - 515	Deformation vibrations of the Si–O–Si bridges.

Table 6 FTIR peaks and characteristics of doped glass.

Sl no.	Wave number (cm^{-1})	Characteristics
1	3467 - 3469	Stretching of O–H– bond inside the glassy network**.**
2	1200 - 1750	Asymmetric stretching relaxation of the B-O bonds of trigonal BO_3 units.
3	1200 - 1750	Asymmetric stretching relaxation of the B-O bond of trigonal BO_3 units.
4	1200 - 1750	Asymmetric stretching relaxation of the B-O bond of trigonal BO_3 units.
5	990 - 1000	Stretching vibration of Si-O-Si linkage.
6	704 - 715	Bonding of B-O-B linkages (diborate linkage).
7	470 - 520	Vibrations of metal cations such as Ba^{2+}.

5.3 DIFFERENTIAL SCANNING CALORIMETRY (DSC)

The DSC study of base glass samples having composition $[(BaZr_{0.1}Ti_{0.9}O_3]$-$[2SiO_2$-$B_2O_3]$-$[K_2O]$ was done from room temperature to 700˚C and for doped glass sample having composition $[(BaZr_{0.1}Ti_{0.9}O_3]$-$[2SiO_2$-$B_2O_3]$-$[K_2O]$-0.1 mol.% La_2O_3 from room temperature to 750ºC at a heating rate of 10˚Cmin^{-1}.

DSC trace of base glass quenched on a pre-heated graphite plate is shown in **Fig. 5.1.1**. This graph shows crystallization of glass (Tc) at a peak 560˚C. Another peak from the curve can be seen at 630˚C. The onset of crystallization (T_x) was found to be 480˚C. Therefore the temperature between 480˚C and 560˚C was chosen for making glass ceramics since there will be no crystallization below 480˚C and after 560˚C crystallization will be completed. The glass transition temperature (T_g) was found to be 300˚C. So, the glass stability factor (T_x - T_g) = 180˚C.

DSC trace of base glass quenched at room temperature is shown in **Fig. 5.1.2**. This graph shows crystallization of glass (Tc) at a peak 605˚C. The onset of crystallization (T_x) was found to be 564ºC. Therefore the temperature between 564˚C and 605˚C was chosen for making glass ceramics since there will be no crystallization below 564˚C and after 605˚C crystallization will be completed. The glass transition temperature (T_g) was found to be 315˚C. So, the glass stability factor (T_x - T_g) = 249˚C.

DSC trace of doped glass quenched at room temperature is shown in **Fig. 5.1.3**. This graph shows crystallization of glass (Tc) at a peak 620˚C. Another peak from the curve can be seen at 690˚C. The onset of crystallization (T_x) was found to be 530˚C. Therefore the temperature between 530˚C and 620˚C was chosen for making glass ceramics since there will be no crystallization below 530˚C and after 620˚C crystallization will be completed. The glass transition temperature (T_g) was found to be 328˚C. So, the glass stability factor (T_x - T_g) = 202˚C

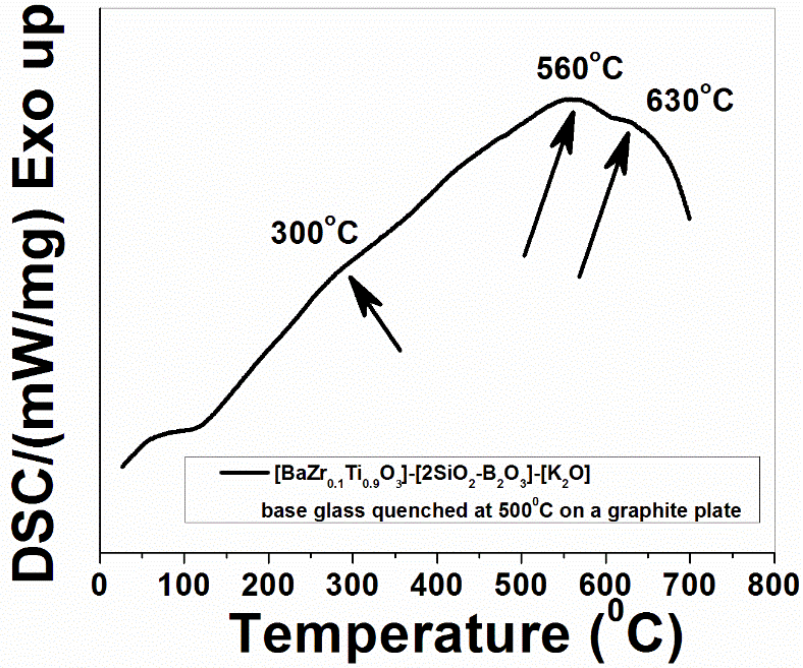

Fig. 5.3.1 DSC study from room temperature to 700˚C for base glass quenched at 500˚C on a graphite plate.

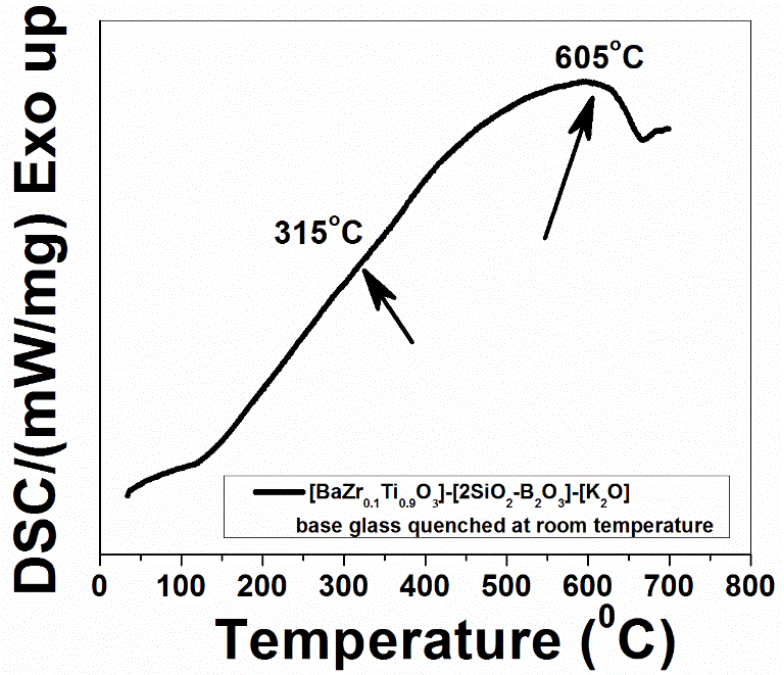

Fig. 5.3.2 DSC study from room temperature to 700˚C for base glass quenched at room temperature.

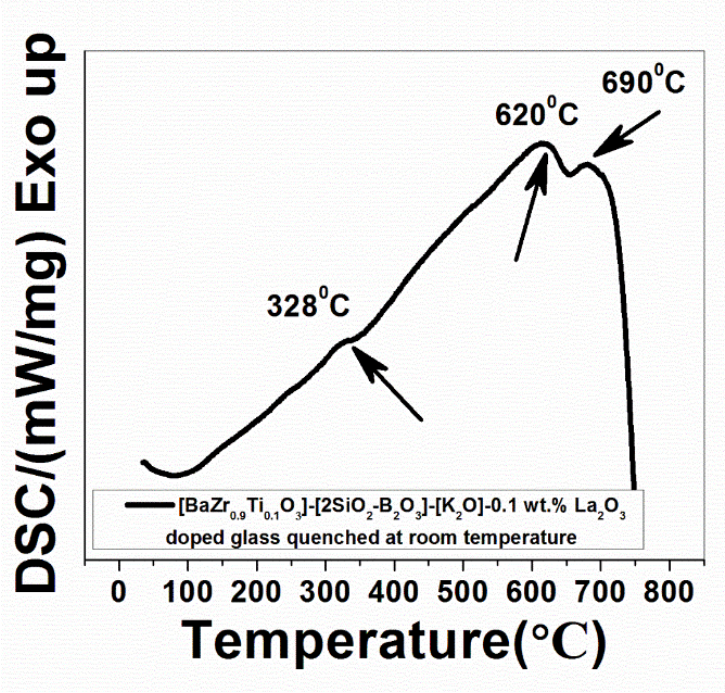

Fig. 5.3.3 DSC study from room temperature to 750˚C for doped glass quenched at room temperature.

5.4 DENSITY MEASUREMENT

Density was measured for four samples by calculating bulk density for base glass having composition $[(BaZr_{0.1}Ti_{0.9}O_3]$-$[2SiO_2$-$B_2O_3]$-$[K_2O]$ and doped glass having composition $[(BaZr_{0.1}Ti_{0.9}O_3]$-$[2SiO_2$-$B_2O_3]$-$[K_2O]$-0.1 mol.% La_2O_3 as shown in **Table 7** and **Table 8,** respectively. From the aforementioned tables it could be very well observed the density of glass ceramic samples are slightly higher than the glass samples. Because they have been transformed from an amorphous structure to a crystalline structure. The growth and formation of crystals in-between the samples increases the density of the glass ceramic samples with the addition of 0.1 mol.% La_2O_3. With the increase of the dwelling time the crystal size increases which results in the increase in density of the glass ceramic.

Table 7 Density measurement of the glass samples.

Glass samples	Dry weight (D) gm	Suspended weight (S) gm	Soaked weight (W) gm	Bulk density = D(W-S)	Average in (g/cc)
Base glass (quenched at high temperature)	1. 3.2676	1. 2.2247	1. 3.2860	1. 3.1320	
	2. 1.9157	2. 1.3050	2. 1.9160	2. 3.1353	3.1402 ± 0.01
	3. 1.8630	3. 1.2725	3. 1.8633	3. 3.1533	
Doped glass (quenched at room temperature)	1. 0.8689	1. 0.6204	1. 0.8701	1. 3.4798	
	2. 0.8078	2. 0.5765	2. 0.8079	2. 3.4954	3.4944 ± 0.01
	3. 3.6655	3. 2.6213	3. 3.6662	3. 3.5080	

Table 8 Density measurement of the glass ceramic samples (after crystallization).

Glass Ceramic samples	Dry weight (D) gm	Suspended weight (S) gm	Soaked weight (W) gm	Bulk density = D/(W-S)	Average in (g/cc)
Base glass (quenched at high temperature)	1. 0.6398	1. 0.4371	1. 0.6408	1. 3.1409	
	2. 0.5976	2. 0.4103	2. 0.5998	2. 3.1536	3.153 ± 0.01
	3. 0.3731	3. 0.2558	3. 0.3737	3. 3.1645	
Doped glass (quenched at room temperature)	1. 0.9691	1. 0.69216	1. 0.9694	1. 3.4955	
	2. 0.7578	2. 0.5423	2. 0.7581	2. 3.5130	3.5049 ± 0.01
	3. 0.8022	3. 0.5738	3. 0.8025	3. 3.5071	

5.5 X-RAY DIFFRACTION (XRD) OF GLASS CERAMIC

Glass ceramic samples were ground to fine powder for XRD analysis. **Fig. 5.5.1-5.5.2** shows the XRD plot of each samples having the compositions [($BaZr_{0.1}Ti_{0.9}O_3$]-[$2SiO_2$-B_2O_3]-[K_2O] quenched on a preheated plate graphite plate and the doped glass [($BaZr_{0.1}Ti_{0.9}O_3$]-[$2SiO_2$-B_2O_3]-[K_2O] - 0.1 mol. % La_2O_3 quenched at room temperature respectively. After controlled heat treatment the glass samples were crystallized and had turned from glass to glass ceramics. The glass samples had turned to glass ceramics is confirmed only through XRD analysis. The **Fig. 5.5.1**

shows the formation of fresnoite $Ba_2TiSi_2O_8$ phase in base glass sample upon crystallization which is confirmed through the JCPDS file. Lattice parameter(s) were calculated by least-square technique. Calculated Lattice parameter(s) of the sample [a = 0.852408 nm, c = 0.520981 and unit cell volume = 378.5444 * 10^{-3} nm^3] matched quite well with the standard lattice cell parameter(s) [a = 0.8527 nm c = 0.521nm and unit cell volume = 378.82 * 10^{-3} nm^3] of $Ba_2TiSi_2O_8$ phase. The **Fig. 5.5.2** shows the formation of fresnoite ($Ba_2TiSi_2O_8$) phase in the glass ceramic sample which is confirmed through the JCPDS file. Lattice parameter(s) were calculated by least-square technique. Calculated Lattice parameter(s) of the sample [a = 0.846456 nm, c = 0.515724 and unit cell volume = 369.5099 * 10^{-3} nm^3]. The calculated lattice parameter matches quite well with the standard lattice parameter of fresnoite phase. Fresnoite phase is formed because the Ba^{2+} ion was not replaced by La^{2+} ion. The crystal system of Fresnoite phase is tetragonal in structure and ferroelectric in nature.

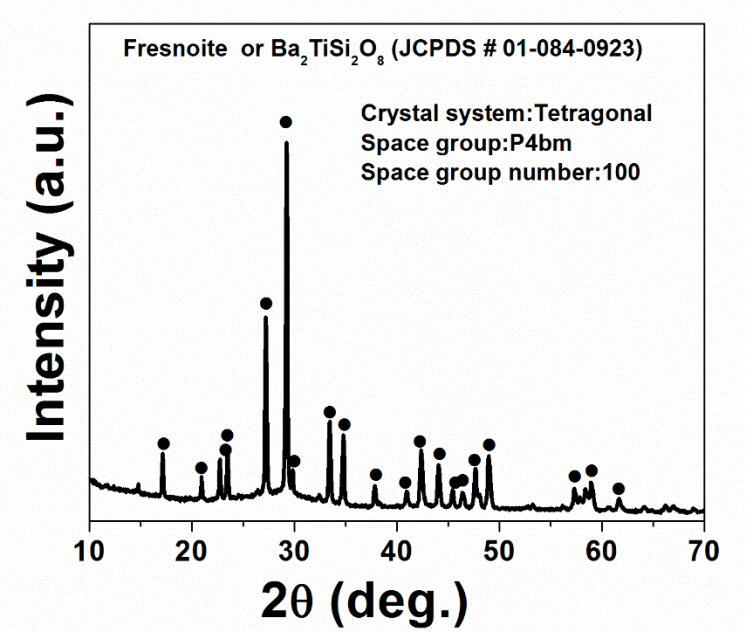

Fig. 5.5.1 XRD analysis of [($BaZr_{0.1}Ti_{0.9}O_3$]-[$2SiO_2$-B_2O_3]-[K_2O] glass ceramic sample.

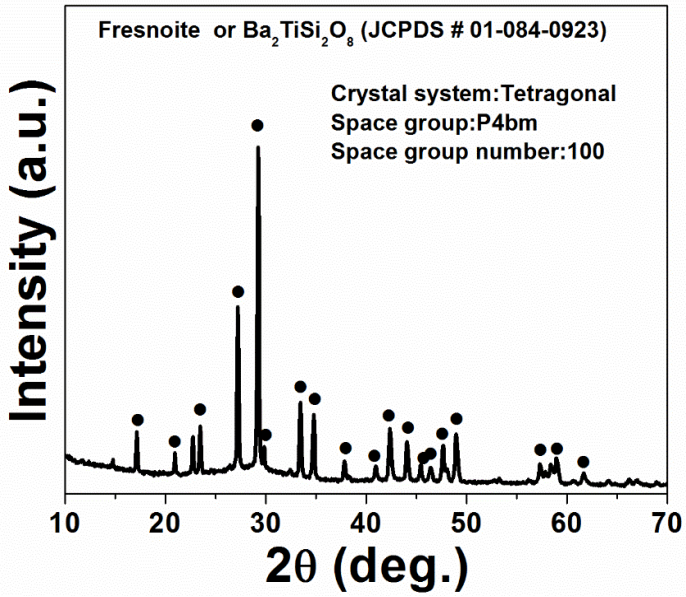

Fig. 5.5.2 XRD analysis of $[(BaZr_{0.1}Ti_{0.9}O_3]$-$[2SiO_2$-$B_2O_3]$-$[K_2O]$ - 0.1 mol. % La_2O_3 glass ceramic sample.

5.6 SCANNING ELECTRON MICROSCOPY (SEM)

SEM showed the detailed microstructural morphology analysis of the samples. Elemental X-Ray mapping results were also obtained which shows the distribution of all the elements present in the microstructure. Energy Dispersive Spectroscopy (EDS) results obtained shows the quantitative analysis of the microstructures present in the samples. The surface morphology of BZT base glass ceramic having the composition $[(BaZr_{0.1}Ti_{0.9}O_3]$-$[2SiO_2$-$B_2O_3]$-$[K_2O]$ quenched on a preheated plate graphite plate and the doped glass ceramic having the composition $[(BaZr_{0.1}Ti_{0.9}O_3]$-$[2SiO_2$-$B_2O_3]$-$[K_2O]$ - 0.1 mol. % La_2O_3 quenched at room temperature were observed.

The **Fig. 5.6.1** shows the surface morphology of base glass ceramic sample. The mophology shows three types of crystal formed they are L-shaped matrix, needle shaped crystals and square with hole are present throughout the microstructure after controlled crystallization. EDS analysis as shown in **Fig. 5.6.2** suggests that the L-shaped crystals are Ba, Ti, Si and O rich.

It is likely that Fresnoite $Ba_2TiSi_2O_8$ phase has been formed. EDS analysis of matrix of base glass ceramic sample as shown in **Fig. 5.6.3** suggests that it is rich in O, K, Si, and Ti. The **Fig. 5.6.4** shows the EDS analysis of needle-like crystals present throughout the microstructure of the base glass sample. Some secondary phase rich in Ti, Si, O, B, K has been formed. EDS analysis as shown in **Fig. 5.6.5** suggests that square crystals are Ba, Ti, Si and O rich. It is likely that Fresnoite $Ba_2TiSi_2O_8$ phase has been formed. **Fig. 5.6.6** shows Elemental X-Ray mapping of base glass ceramic sample. X-ray elemental mapping reveals that L-shaped crystals are Titanium and Barium rich composition. Potassium is rich in the matrix. Oxygen, Silicon, Zirconium, Boron are equally distributed.

The **Fig. 5.6.7** shows the surface morphology of 0.1 mol % La_2O_3 doped glass ceramic sample. Blocky and globular crystals and fine interconnected precipitates are observed throughout the microstructure after controlled crystallization. EDS analysis as shown in **Fig. 5.6.8** to **Fig.5.6.10** suggests that globular crystals, fine interconnected precipitates and the matrix are B and O rich. Elemental X-Ray mapping as shown in **Fig. 5.6.11** for doped glass ceramic sample reveals that the sample is rich in Boron and Oxygen throughout the microstructure after crystallization.

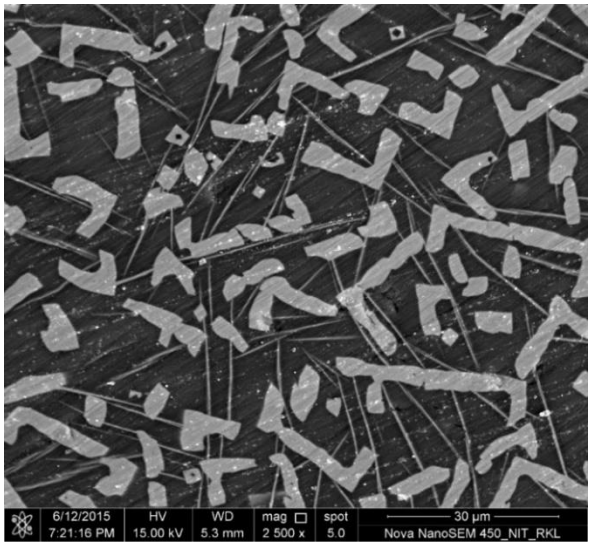

Fig. 5.6.1 SEM image of base glass ceramic sample.

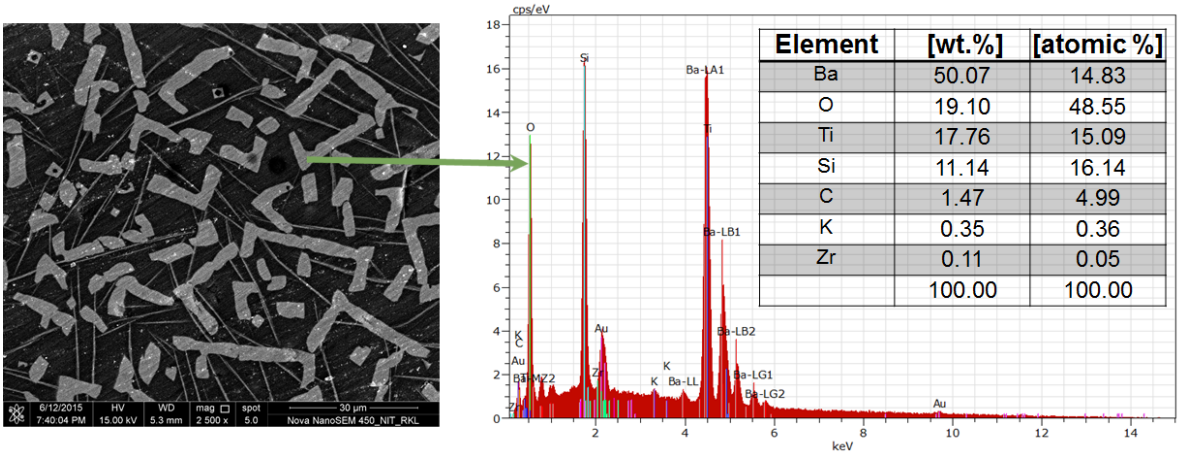

Element	[wt.%]	[atomic %]
Ba	50.07	14.83
O	19.10	48.55
Ti	17.76	15.09
Si	11.14	16.14
C	1.47	4.99
K	0.35	0.36
Zr	0.11	0.05
	100.00	100.00

Fig. 5.6.2 EDS analysis of L-shaped crystals in the microstructure of base glass ceramic sample.

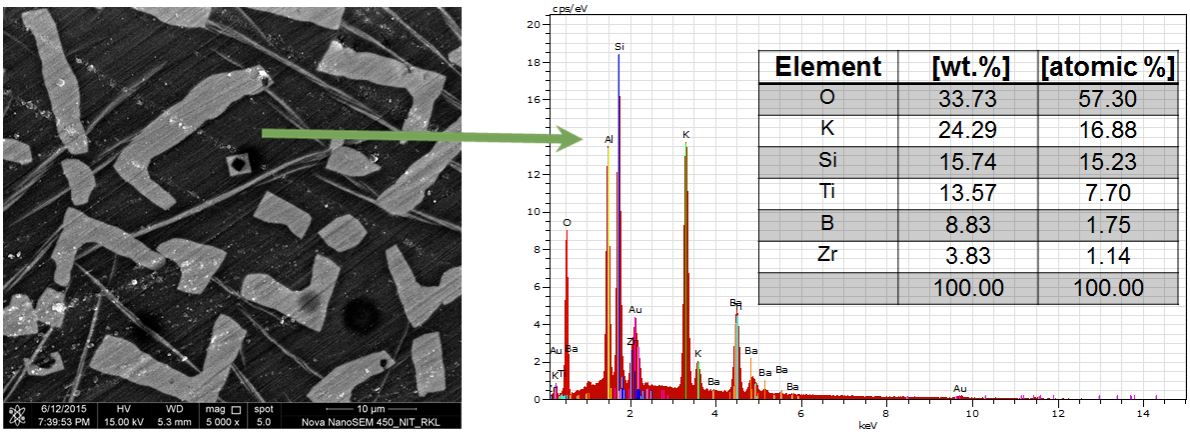

Element	[wt.%]	[atomic %]
O	33.73	57.30
K	24.29	16.88
Si	15.74	15.23
Ti	13.57	7.70
B	8.83	1.75
Zr	3.83	1.14
	100.00	100.00

Fig. 5.6.3 EDS analysis of matrix in the microstructure of base glass ceramic sample.

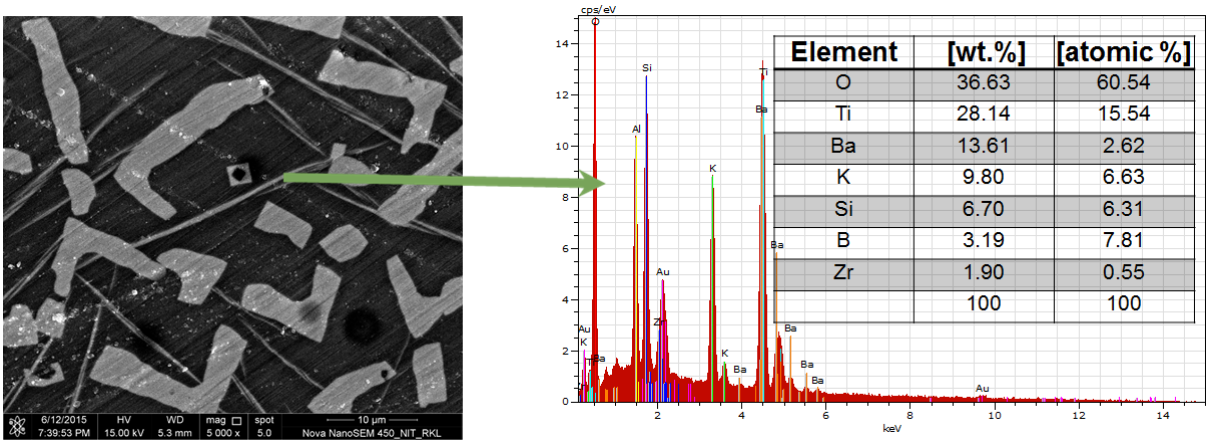

Element	[wt.%]	[atomic %]
O	36.63	60.54
Ti	28.14	15.54
Ba	13.61	2.62
K	9.80	6.63
Si	6.70	6.31
B	3.19	7.81
Zr	1.90	0.55
	100	100

Fig. 5.6.4 EDS analysis of needle-like crystals in the microstructure of base glass ceramic sample.

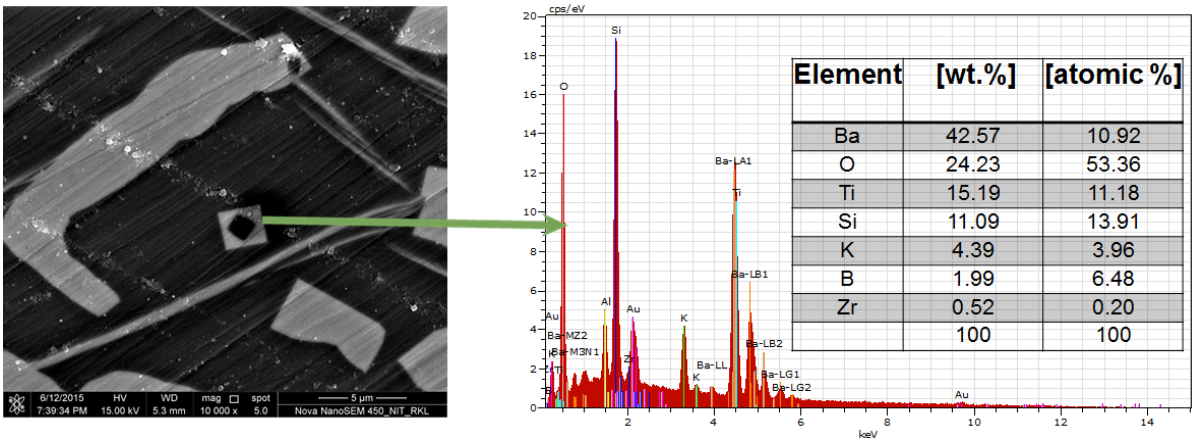

Fig. 5.6.5 EDS analysis of square crystal in the microstructure of base glass ceramic sample.

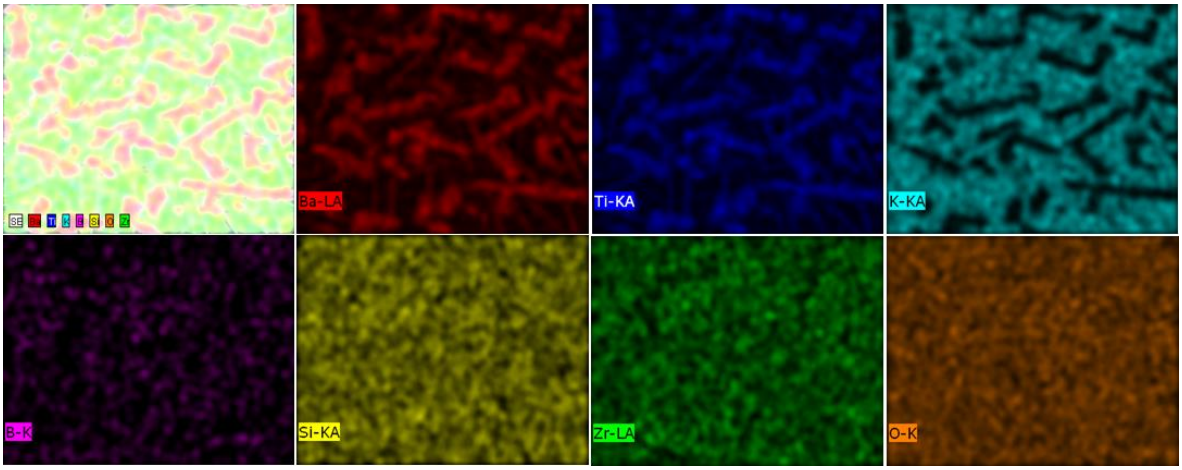

Fig. 5.6.6 Elemental X-Ray mapping of base glass ceramic sample.

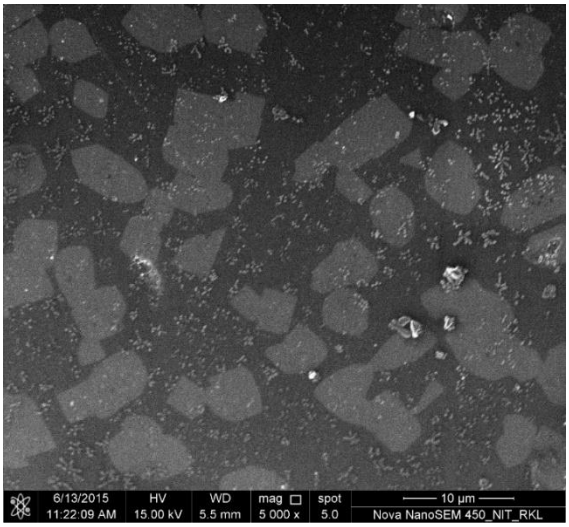

Fig. 5.6.7 SEM image of doped glass ceramic sample.

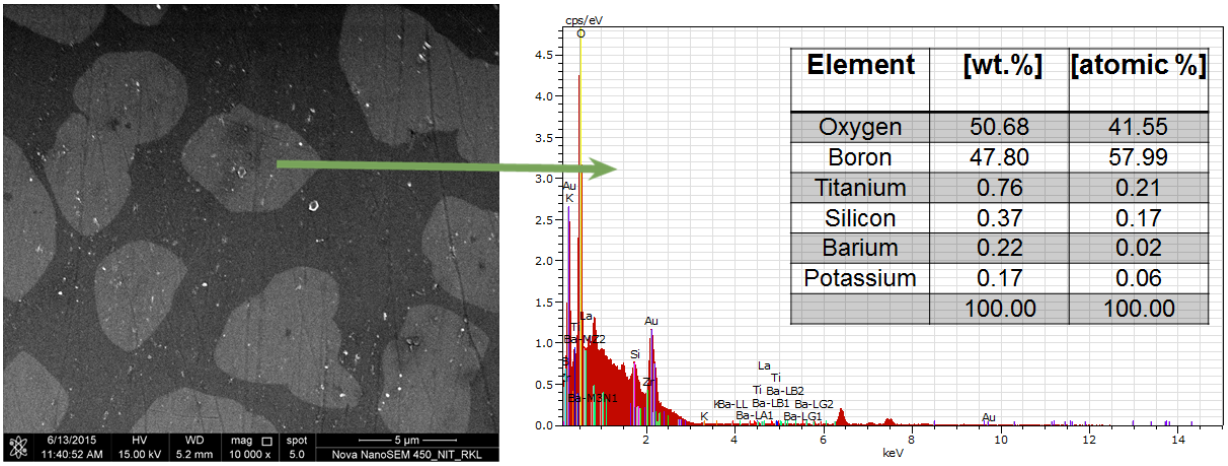

Element	[wt.%]	[atomic %]
Oxygen	50.68	41.55
Boron	47.80	57.99
Titanium	0.76	0.21
Silicon	0.37	0.17
Barium	0.22	0.02
Potassium	0.17	0.06
	100.00	100.00

Fig. 5.6.8 EDS analysis of blocky and globular crystals in the microstructure of doped glass ceramic sample.

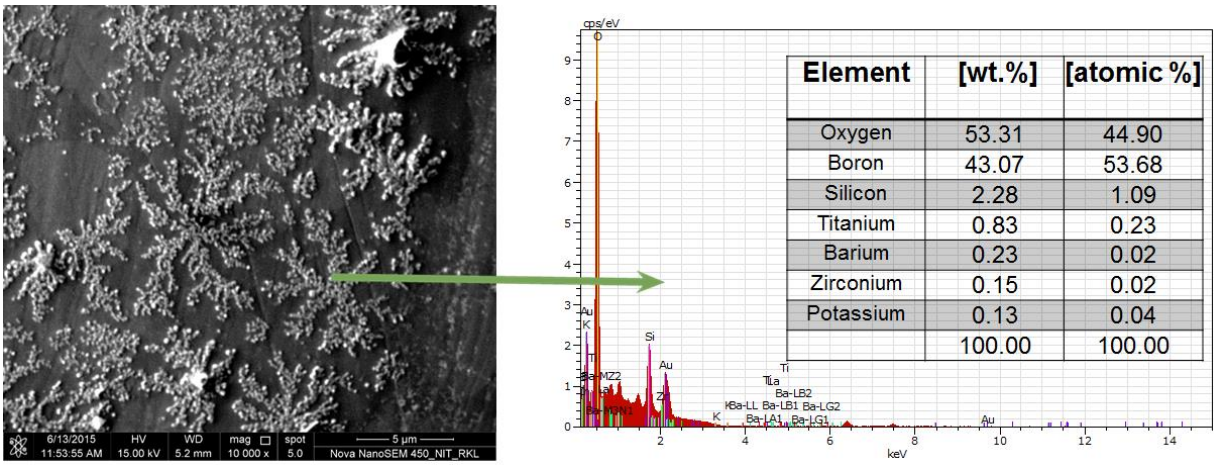

Element	[wt.%]	[atomic %]
Oxygen	53.31	44.90
Boron	43.07	53.68
Silicon	2.28	1.09
Titanium	0.83	0.23
Barium	0.23	0.02
Zirconium	0.15	0.02
Potassium	0.13	0.04
	100.00	100.00

Fig. 5.6.9 EDS analysis of fine interconnected precipitates in the microstructure of doped glass ceramic sample.

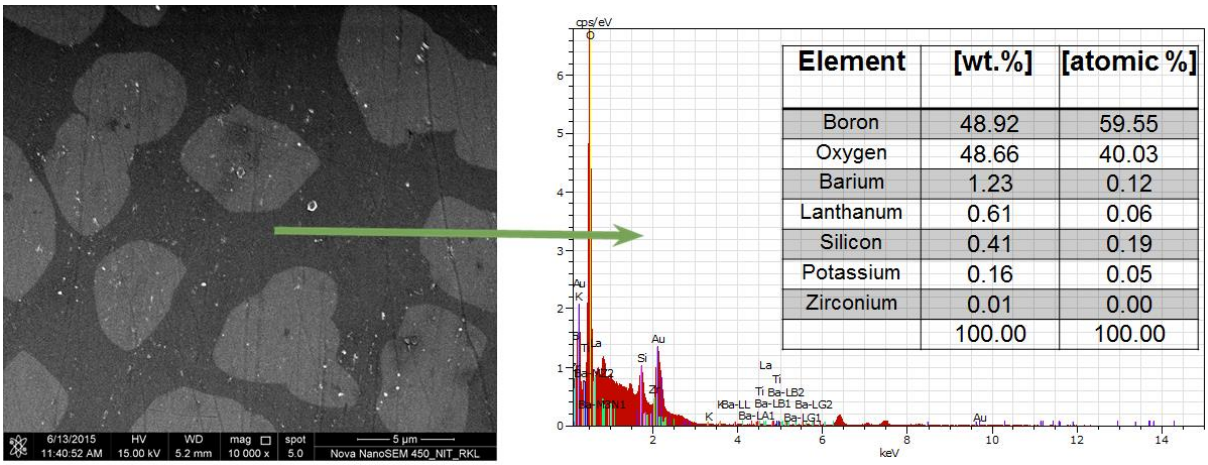

Element	[wt.%]	[atomic %]
Boron	48.92	59.55
Oxygen	48.66	40.03
Barium	1.23	0.12
Lanthanum	0.61	0.06
Silicon	0.41	0.19
Potassium	0.16	0.05
Zirconium	0.01	0.00
	100.00	100.00

Fig. 5.6.10 EDS analysis of matrix in the microstructure of doped glass ceramic sample.

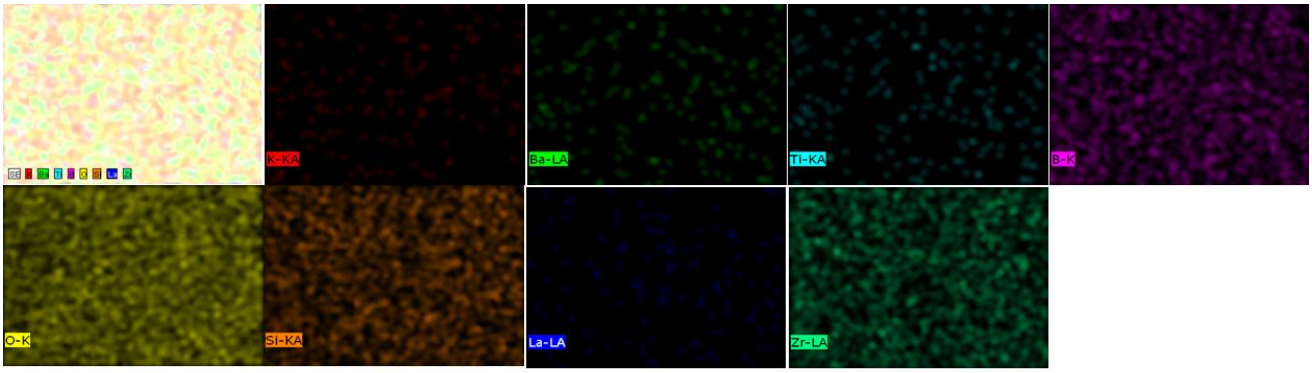

Fig. 5.6.11 Elemental X-Ray mapping of doped glass ceramic sample.

5.7 DIELECTRIC ANALYSIS

The dielectric properties of glass ceramics are controlled by factors such as the crystallite size, morphology, nature and amount of crystalline phases. Dielectric properties also depends on crystal clamping, secondary phases and the connectivity of the high permittivity perovskite crystals in the low permittivity glassy matrix. The nature of micro-structure and crystalline phases of glass ceramics can be controlled in the heat treatment conditions. The dielectric measurement at room temperature with varying frequency was analyzed.

As shown in **Fig. 5.7.1** for base glass ceramic sample having composition [($BaZr_{0.1}Ti_{0.9}O_3$]-[$2SiO_2$-B_2O_3]-[K_2O] quenched at high temperature on a pre-heated graphite plate and crystallized at 800^oC the dielectric measurement was done at room temperature with varying frequency. Dielectric constant measured at room temperature remains constant (~45) with the measured frequencies (100 Hz, 1 kHz, 10 kHz, 100 kHz, and 1 MHz). Loss is < 0.05 from 300 kHz to 1MHz. However the Loss is >0.05 in the frequency range 100 Hz to 300 kHz. Dielectric dispersion is very small in the frequency range 10 kHz to 1 MHz.

The **Fig. 5.7.2** shows the dielectric measurement done at room temperature for doped glass ceramic sample having composition [($BaZr_{0.1}Ti_{0.9}O_3$]-[$2SiO_2$-B_2O_3]-[K_2O]-0.1 wt.% La_2O_3

quenched at room temperature and crystallized at 800°C. Dielectric constant measured at room temperature remains constant (~125) with the measured frequencies (100 Hz, 1 kHz, 10 kHz, 100 kHz, and 1 MHz). Loss is very low < 0.05 and same as that of base glass ceramic sample from 100 Hz to 1 MHz. Very small dielectric dispersion in the frequency range 100 kHz to 1MHz. Dielectric constant increases with 0.1 mol.% La_2O_3 doping in the BZT glass ceramics.

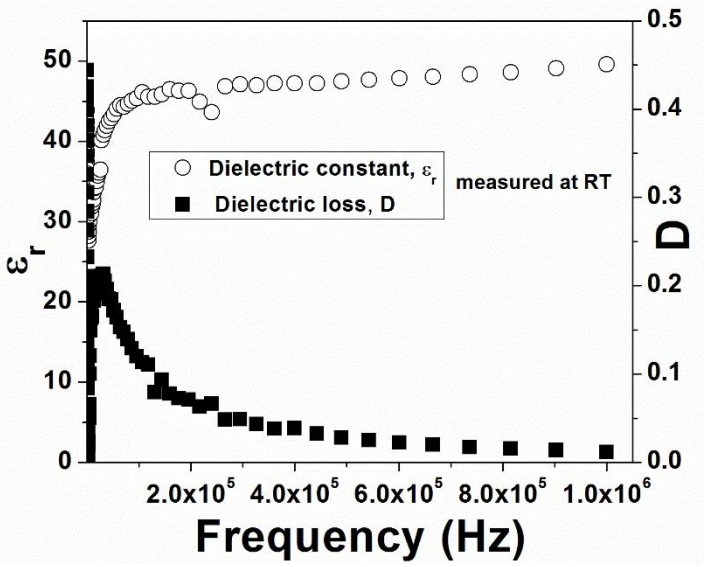

Fig. 5.7.1 Dielectric measurement of base glass ceramic sample at room temperature with variation of frequency.

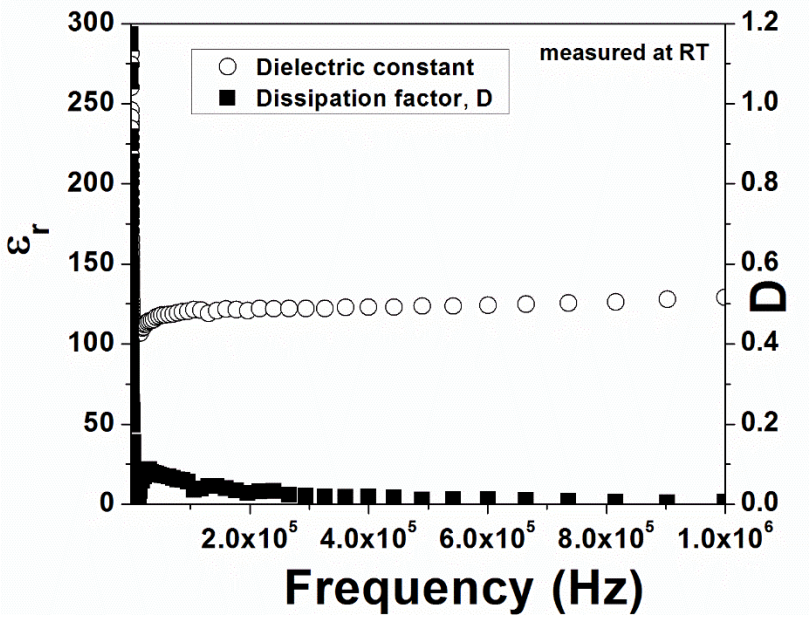

Fig. 5.7.2 Dielectric measurement of doped glass ceramic sample at room temperature with variation of frequency.

6. CONCLUSION

- BZT glass was successfully synthesized using melt-quench method.
- FTIR spectra of base glass and 0.1 mol.% La_2O_3 doped glass shows the presence of stretching vibration of O–H bond inside the glassy network. Asymmetric stretching of B–O bond, stretching vibrations of B- O-Si linkage and deformation vibrations of the Si–O–Si bridges were also observed.
- DSC scan of base glass and doped glass reveals that addition of 0.1 mol.% La_2O_3 into BZT base glass composition elevates the glass transition and onset of crystallization temperature.
- XRD analysis of base glass and doped glass sample shows broad peaks around ~24-35^0 (2θ value) which is due to the formation of amorphous borosilicate phase. The presence of amorphous borosilicate phase confirms formation of glass. XRD analysis of base glass ceramic and doped glass ceramic samples shows the formation of fesnoite- $Ba_2TiSi_2O_8$ phase upon crystallization at 800^{0}C for 3h in air.
- SEM shows the formation of micron sized L-shaped Fresnoite crystals in the base glass ceramic sample. EDS confirms the composition is $Ba_2TiSi_2O_8$. Addition of 0.1 mol.% La_2O_3 modifies the L-shaped crystals to blocky and globular crystals.
- Dielectric measurement shows the dielectric constant improves from ~45 to ~125 with the addition of 0.1 mol.% La_2O_3 into the BZT glass ceramic.

7. REFERENCE

1. C. E. Ciomaga, R. Calderoneb, M. T. Buscagliac, M. Vivianic, V. Buscaglia, L. Mitoseriua,B,A. Stancua, P. Nannib "Relaxor Properties Of Ba(Zr,Ti)O_3 Ceramics", *J. Optoelec Adv. Mater,* 8, No. 3, (2006), p. 944 - 948
2. B. Wul and I. M. Goldman, C. R. Acad. Sci. U. R. S. S. 46, 177 (1945).
3. M. E. Lines and A. M. Glass, Principles and Applications of Ferroelectrics and Related Materials, Clarendon Press, Oxford, (1977)
4. Xiangrong Wang, Yong Zhang *, Ivan Baturin , Tongxiang Liang, "Blocking effect of crystal–glass interface in lanthanum doped barium strontium titanate glass ceramics", *Materials Research Bulletin*, 48, (2013), p. 3817–3821
5. Xiujian Chou, Jiwei Zhai ∗, Xi Yao, "Relaxor behavior and dielectric properties of La_2O_3-doped barium zirconium titanate ceramics for tunable device applications", *Materials Chemistry and Physics*, 109, (2008), p. 125–130
6. Feri Adriyanto, Chih-Kai Yang, Tsung-Yu Yang, Chia-Yu Wei, and Yeong-Her Wang, "Solution-Processed Barium Zirconate Titanate for Pentacene-Based Thin-Film Transistor and Memory" *IEEE Electron Device Letters*, 34, 10, (2013), p. 1241-1243
7. Tanmoy Maiti, R. Guo, and A. S. Bhalla, "Structure-Property Phase Diagram of $BaZr_xTi_{1-x}O_3$" *J. Am. Ceram. Soc.*, 91, 6, (2008), p 1769–1780
8. F. Mouraa, A.Z. Simoes, B.D. Stojanovic, M.A. Zaghete, E. Longoa, J.A. Varela, "Dielectric and ferroelectric characteristics of barium zirconate titanate ceramics prepared from mixed oxide method" *J. of Alloys & Compounds*, 462, 1–2, 25, (2008), p. 129–134
9. S. Sarangi, T. Badapanda, B. Behera, S. Anwar, "Frequency and temperature dependence dielectric behavior of barium zirconate titanate nanocrystalline powder obtained by mechano-chemical synthesis" *J Mater Sci: Mater Electron*, (2013) 24, p. 4033–4042
10. P. G. Bray, "Interaction of Radiation with Solids," Plenum, New York, 1967
11. N. A. Ghoneim, H. A. El Batal, N. Abdel Shafi and M. H. Azooz, "Synthesis and Characterization of Cadmium Doped Lead-Borate Glasses, "*Proceeding of the Egyptian Conference of Chemistry*", Cairo, 1996, p. 162
12. A. S. Tenny and J. J. Wong, "Vibrational Spectra of Vapour Deposited Binary Borosilicate Glasses, "*Chemical Physics*", Vol. 56, No. 11, (1972), p. 5516-5523

13. H. Doweidar, M. A. A. Zeid and G. M. El-Damrawy, "Effect of Gamma Radiation and Thermal Treatment on Some Physical Properties of ZnO-PbO-B_2O_3 Glasses, "*Journal of Physics D*, 24, 12, (1991), p. 2222- 2228
14. Chandkiram Gautam, Avadhesh Kumar Yadav, Vijay Kumar Mishra, Kunwar Vikram, "Synthesis, IR and Raman Spectroscopic Studies of (Ba,Sr)TiO_3 Borosilicate Glasses with Addition of La_2O_3" *Open Journal of Inorganic Non-metallic Materials*, 2, 4,(2012), p. 47-54